# The thermal and dynamical state of the atmosphere during polar mesosphere winter echoes

F.-J. Lübken, B. Strelnikov, M. Rapp, W. Singer, R. Latteck, A. Brattli, U.-P. Hoppe, M. Friedrich

HAL Id: hal-00301733

https://hal.science/hal-00301733

Submitted on 18 Jun 2008

**Atmospheric
Chemistry
and Physics
Discussions**

Polar mesosphere
winter echoes

F.-J. Lübken et al.

Title Page

| Abstract | Introduction |
|---|---|
| Conclusions | References |
| Tables | Figures |

| ◄◄ | ►► |
|---|---|
| ◄ | ► |
| Back | Close |

Full Screen / Esc

Print Version

Interactive Discussion

EGU

# The thermal and dynamical state of the atmosphere during polar mesosphere winter echoes

F.-J. Lübken[1], B. Strelnikov[1], M. Rapp[1], W. Singer[1], R. Latteck[1], A. Brattli[2],
U.-P. Hoppe[2], and M. Friedrich[3]

[1]Leibniz Institute of Atmospheric Physics, Kühlungsborn, Germany
[2]Norwegian Defence Research Establishment (FFI), Kjeller, Norway
[3]Institute of Communications Networks and Satellite Communications, Graz University of
Technology, Austria

Correspondence to: F.-J. Lübken (luebken@iap-kborn.de)

Title Page

Abstract · Introduction

Conclusions · References

Tables · Figures

◄ · ►►

◄ · ►

Back · Close

Full Screen / Esc

Print Version

Interactive Discussion

[EGU](#)

## Abstract

In January 2005, a total of 18 rockets were launched from the Andøya Rocket Range in Northern Norway (69° N) into strong VHF radar echoes called 'Polar Mesosphere Winter Echoes' (PMWE). The echoes were observed in the lower and middle mesosphere during large solar proton fluxes. In general, PMWE are much more seldom compared to their summer counterparts PMSE (typical occurrence rates at 69° N are 1–3% vs. 80%, respectively). Our in-situ measurements by falling sphere, chaff, and instrumented payloads provide detailed information about the thermal and dynamical state of the atmosphere and therefore allow an unprecedented study of the background atmosphere during PMWE. There are a number of independent observations indicating that neutral air turbulence has caused PMWE. Ion density fluctuations show a turbulence spectrum within PMWE and no fluctuations outside. Temperature lapse rates close to the adiabatic gradient are observed in the vicinity of PMWE indicating persistent turbulent mixing. The spectral broadening of radar echoes is consistent with turbulent velocity fluctuations. Turbulence also explains the mean occurrence height of PMWE (∼68–75 km): Viscosity increases rapidly with altitude and destroys any small scale fluctuations in the upper mesosphere, whereas electron densities are usually too low in the lower mesosphere to cause significant backscatter. The seasonal variation of echoes in the lower mesosphere is in agreement with a turbulence climatology derived from earlier sounding rocket flights. We have performed model calculations to study the absolute magnitude of backscatter from plasma fluctuations caused by neutral air turbulence. We find that volume reflectivities observed during PMWE are in quantitative agreement with theory. Apart from turbulence the most crucial requirement for PMWE is a sufficiently large number of electrons, for example produced by solar protons. We have studied the sensitivity of the radar echo strength on various parameters, most important electron number density and turbulence intensity. Our observational and theoretical considerations do not provide any evidence that charged aerosol particles are needed to explain PMWE, in contrast to the summer echoes which owe their

existence to charged ice particles.

## 1. Introduction

The existence and the properties of radar echoes can provide important information about the background atmosphere, for example on winds and turbulence. It is there-
fore crucial to understand their physical origin. It has become clear in recent years that VHF radar echoes from the summer mesopause region at mid and high latitudes are directly linked to charged ice particles which implies that temperatures are lower than ~150 K. These radar echoes are called (polar) mesosphere summer echoes, (P)MSE, and were first observed in the late 1970's (Czechowsky et al., 1979). A review on obser-
vations and our current understanding of PMSE has recently been published by Rapp and Lübken (2004). Occasionally, strong radar echoes have also been observed in the winter mesosphere and were later called 'polar mesosphere winter echoes', PMWE (Czechowsky et al., 1979; Ecklund and Balsley, 1981; Kirkwood et al., 2002). Since at-
mospheric temperatures are generally much too high in the winter mesosphere to allow
the existence of ice particles, Stebel et al. (2004) speculate that small charged aerosol particles (other than ice) are present and influence the plasma such that radar echoes can occur. The winter echoes are much less frequent than their summer counterparts (occurrence rates of 1–3% and ~80%, respectively, at polar latitudes). This makes it extremely difficult to experimentally determine their characteristics and to study the
physical processes involved. PMWE appear approximately between 55 and 80 km with a maximum occurrence around 68–75 km (see Zeller et al., 2005[1], for more details). Nearly all of these echoes have been observed when the Sun photo-ionizes the meso-
sphere and when solar and/or geomagnetic activity provides an additional source of electrons.

---

[1]Zeller, O., Zecha, M., Bremer, J., Latteck, R., and Singer, W.: Mean characteristics of meso-
sphere winter echoes at mid and high latitudes, J. Atmos. Solar Terr. Phys., to be submitted, 2005.

**Polar mesosphere winter echoes**

F.-J. Lübken et al.

Title Page

| Abstract | Introduction |
| Conclusions | References |
| Tables | Figures |

◄◄ ►►

◄ ►

Back Close

Full Screen / Esc

Print Version

Interactive Discussion

EGU

In January 2005 we launched a sequence of meteorological and instrumented rockets into PMWE at high latitudes. Considering the very low occurrence rate of PMWE this opportunity was due to very favorable circumstances. These new measurements provide unique information about the conditions in the neutral and charged atmosphere. In this paper we summarize the temperature and wind measurements of the meteorological rockets (falling sphere and chaff) and provide some important results from the instrumented rockets. We will present observational and theoretical evidence that neutral air turbulence alone (i.e., without the presence of charged aerosols) can create PMWE.

## 2. The ROMA/PMWE campaign

In January 2005 a series of rockets were launched from the Andøya Rocket Range (69°) while the co-located ALWIN VHF radar detected strong echoes in the mesosphere. This campaign was part of a project called 'Rocket borne Observations in the Middle Atmosphere' (ROMA). The dates and times of rocket launches are listed in Table 1. The ALWIN radar is part of the ALOMAR observatory (Arctic lidar observatory for middle atmosphere research) and is described in more detail elsewhere (Latteck et al., 1999). The radar operates at 53.5 MHz which corresponds to a Bragg scale of $\ell_{Br} = \lambda/2 \sim 3$ m. The power-aperture product of the radar is $5.3 \cdot 10^7$ W·m$^2$ and the two-way beam halfwidth is 2.55°. Only the vertical beam is available during the winter period. In Fig. 1 the radar signal on 20 January 2005 is shown, when a series of 5 falling spheres were launched. A strong PMWE is observed with maximum backscattered power of more than 24 dB above noise. The echoes come from an altitude range of roughly 55 to 75 km, in agreement with typical occurrence heights.

In Fig. 2 typical profiles of volume reflectivity for winter (PMWE) and summer (PMSE) echoes are shown. As can be seen from this figure the winter echoes are weaker and lower compared to summer ($\eta \sim 10^{-15}$/m at 60–70 km, relative to $10^{-12}$ at 82–90 km, respectively). In both cases the echoes have been integrated for approximately 1/2 h.

As can be seen from Fig. 1 the echoes in the period shown in Fig. 2 are rather strong and can be significantly weaker. We summarize that typical PMWE strengths are on the order of $10^{-16}$–$10^{-15}$/m during our campaign.

A total of 17 falling spheres, 4 chaff, and 2 instrumented rockets were launched from 18 to 27 January, most of them (12, 4, 2, respectively) during PMWE. On 25 and 27 January, i.e., during the last five rocket launches, the ALWIN radar did not detect any PMWE.

We will present only the main idea of the various in-situ experiments since they have been described in more detail elsewhere (Widdel, 1990; Schmidlin, 1991; Lübken, 1999; Friedrich et al., 2004; Brattli et al., 2005[2]). From the falling sphere technique (FS), mass densities, temperatures, and horizontal winds from 95 to 35 km are derived using the deceleration and horizontal deflection of an inflated Mylar sphere which is transported to the lower thermosphere by a small rocket. The altitude resolution is 1–5 km depending on the altitude. The chaff technique relies on a foil cloud consisting of several thousands of small aluminum strips slowly drifting through the atmosphere. This gives horizontal winds with much better resolution compared to FS, but in a rather limited height range of typically 15–20 km.

Electron density profiles were measured using a rocket borne radio wave propagation experiment based on the Faraday rotation/differential absorption technique (see e.g., Mechtly et al., 1967). Because of the large electron density only the higher frequency (3.883 MHz) yielded data, whereas 1.3 MHz was already absorbed at the altitude where the antennas deployed.

Ion densities were measured using a positive ion probe (PIP) located in the front of each of the two instrumented payloads. An electric field in a spherical grid rejects electrons and collects positive ions with very high temporal and spatial resolution (2.44 kHz and <1 m, respectively). Mean ion densities are consistent with electron densities

---

[2]Brattli, A., Hoppe, U.-P., Rapp, M., Lübken, F.-J., Singer, W., et al.: In-situ measurements of plasma parameters within polar mesosphere winter echoes, Atmos. Chem. Phys. Discuss., to be submitted, 2005.

obtained from the wave propagation instrument.

It is obvious from the overall appearance statistics of PMWE that a sufficient number of free electrons is required for these echoes. In wintertime these electrons come from solar radiation (as long as the Sun is above the horizon at mesospheric altitudes) and from solar and geomagnetic activity. The latter sources completely dominate over solar radiation during disturbed conditions. During the ROMA/PMWE campaign altitudes above 70 km were sunlit from ∼07:00–15:00 UT (=08:00–16:00 LT). All PMWE observed during our campaign appeared during this time of day. Furthermore, the GOES-11 satellite showed strong energetic proton fluxes in the period 17–21 January which were enhanced by about 3 orders of magnitude compared to quiet conditions. In addition, on January 18 we observed strong riometer absorption (∼3 dB) above our launch site and large fluctuations in magnetometer recordings both at Andenes and Tromsø (ΣK-indices = 54), indicating strong particle precipitation from the magnetosphere. Furthermore, on 20 January a very strong X-ray event of class X7.1 at 1.0–8.0 Å (corresponding to $7.1 \cdot 10^{-4}$ W/m$^2$) was observed by GOES-11. We summarize that the PMWE during our campaign occurred during a period of strong solar and geomagnetic disturbance leading to enhanced electron densities. This scenario supports the observations by Kirkwood et al. (2002), namely that PMWE can occur only if the number density of free electrons, $N_e$, is sufficiently large. We will later demonstrate in more detail the crucial importance of $N_e$ for a quantitative understanding of PMWE and will use measured electron number densities to calculate volume reflectivities.

## 3. Experimental results

In Fig. 3 all 11 temperature profiles measured during PMWE are shown. We allocate the launches on 18, 20, and 21 January as PMWE launches, although during a few of these flights the PMWE had just disappeared or was very weak. We thereby take into account that the horizontal distance between the atmospheric volume measured by the radar (sounding vertically) and the falling spheres and chaff is typically 30–

50 km. There is a clear tendency in the profiles shown in Fig. 3 for a steep temperature gradient in the 50–70 km height range. In some cases the temperature gradient is close to the adiabatic lapse rate. We argue that these steep gradients are an indication of turbulent mixing (see below for more details). In Fig. 3 we also show the mean temperature profile for January from the climatology of Lübken and von Zahn (1991), hereafter referred to as L&vZ. This climatology is based on FS measurements, i.e., on the same experimental technique as used here. The mean temperature gradient at PMWE altitudes is significantly smaller in the L&vZ-climatology compared to the measurements in our campaign. This indicates that the thermal structure during our rocket flights was considerably different compared to the climatological mean. We note, however, that the temperature gradient in the L&vZ climatology is smaller (i.e., more negative) in the 60–70 km altitude range, compared to above and below. Therefore, the atmosphere is closer to instability in this height range. It is important to note that the FS technique is not influenced by the presence of aerosol particles (if there should be any) since they cannot exert a noticeable drag on the sphere. In contrast, temperature profiles deduced from lidar measurements might be influenced by aerosols as has been demonstrated, for example, in Stebel et al. (2004) in their Figs. 3 and 4.

In Fig. 4 we show Richardson numbers $Ri = \omega_B^2/(\partial \overline{u}/\partial z)^2$ calculated from the falling sphere temperatures, and winds from chaff and falling sphere, respectively ($\omega_B$=Brunt-Väisälä frequency; $\overline{u}$ = mean horizontal wind). Since the altitude resolution of the falling sphere winds is significantly poorer compared to chaff, the wind shears are systematically smaller and the Richardson number is larger. As can be seen from Fig. 4 the difference is typically one order of magnitude. This implies that FS winds have to be taken with great care when identifying instability regions as has been done in Kirkwood et al. (2003). Richardson numbers from chaff winds in Fig. 4 are very structured and show layers with small values indicating instability roughly above 70 km. Unfortunately, the chaff profile does not cover the entire range of PMWE. Taking into account the limitations about FS winds mentioned above, we still see that $Ri$ is very small (and even negative) at altitudes around 60 km. We will later come back to a comparison of $Ri$

EGU

with PMWE.

We have used a wavelet analysis to determine power spectral densities (PSD) of relative ion density fluctuations defined as $\Delta N_i = \left(N_i - \langle N_i \rangle\right) / \langle N_i \rangle$, where $N_i$ is ion number density, and $\langle N_i \rangle$ is a running mean of $N_i$ over 6 rocket spin periods (Torrence and Compo, 1998; Strelnikov et al., 2003). Figure 5 shows two spectra from the downleg of flight RWMM01. One of the spectra is from an altitude range within PMWE (58.5–59.0 km), the other from outside PMWE (68.0–68.5 km). Power spectral densities are much larger inside PMWE which implies large fluctuations. The spectrum from inside PMWE shows a slope close to $k^{-5/3}$, compatible with an inertial subrange of a Kolmogorov turbulence spectrum. On the other hand, the PSD from outside PMWE is much smaller and 'flat', basically determined by instrumental noise. The spectra from the second flight (RWMM02, not discussed here) show a similar characteristic behavior. We conclude that spectra of ion density fluctuations are consistent with turbulence inside PMWE, and no turbulence outside.

## 4.  Theory of turbulent PMWE

The theory of coherent radar backscatter from a weakly ionized plasma is summarized in Tatarskii (1961) and yields the following expression for the volume reflectivity:

$$\eta^{coh} = 8\pi^2 \left( \frac{e^2 \, \overline{N_e}}{2 \, \epsilon_\circ \, m_e \, c^2} \right)^2 \cdot \Phi_{Ne}(\kappa) \tag{1}$$

where $e$ is the elementary charge, $\overline{N_e}$ is the mean electron density, $\epsilon_\circ$ is the dielectric constant of vacuum, $m_e$ is the electron mass, $c$ is the speed of light, and $\Phi_{Ne}(\kappa)$ is the three-dimensional power spectral density (PSD) of the relative electron density fluctuations at the radar Bragg wave number $\kappa = 2 \cdot (2\pi/\lambda) = 2\pi/\ell_{Br}$. A general expression for $\Phi_{Ne}$ was given by Driscoll and Kennedy (1985) and was later applied to in-situ measurements of neutral and electron density fluctuations (Lübken et al., 1994; Giebeler,

EGU

1995). At scales within the inertial subrange (and smaller) the following expression for the radar reflectivity was derived:

$$\eta = 16 \cdot \pi^2 \left( \frac{e^2 \, \overline{N_e}}{2 \, \epsilon_\circ \, m_e \, c^2} \right)^2 Q^{9/2} \, A \, N_\vartheta \, \epsilon^{-1/3} \eta_{Kol}^{11/3} \cdot \left( y^{-11/3} + y^{-3} \right) \cdot exp \left\{ -\frac{\alpha}{Q^2 Sc} \left( \frac{3}{2} y^{4/3} + y^2 \right) \right\} \quad (2)$$

where $y = Q^{3/2} \cdot \eta_{Kol} \cdot k$ ($k$ = wavenumber), $\eta_{Kol} = (v^3/\epsilon)^{1/4}$ is the Kolmogorov micro scale, $v$ is the kinematic viscosity of air, $\epsilon$ is the turbulent energy dissipation rate, $N_\vartheta$ is the dissipation rate of fluctuations, Sc=$v/D$ is the Schmidt number, $D$ is the diffusivity of the tracer, and $Q=2$, $A=0.033 \cdot a^2$, $a^2=1.74$, $\alpha=0.83$ are numerical constants. Further explanations on the quantities introduced in Eq. (2) are given in the references mentioned above and in Lübken (1992). Note that the size of the aerosol particles enters through a reduced diffusivity, D, which increases the Schmidt number $Sc = v/D$ to values larger than unity. The normalization of $\Phi_{Ne}$ in Eq. (2) is such that the integral of the PSD gives the total variance of the fluctuations:

$$\langle \vartheta'^2 \rangle = \int_{-\infty}^{\infty} \int_{-\infty}^{\infty} \int_{-\infty}^{\infty} \Phi_{Ne}(\boldsymbol{k}) \, dk_x \, dk_y \, dk_z \quad (3)$$

In Fig. 6 we have plotted various cases of Eq. (2), keeping the energy dissipation rate constant ($\epsilon=0.1$ W/kg) and varying the electron number density $N_e$, the Schmidt number $Sc$, and $N_\vartheta$. As can be seen from this figure the PSD at 3 m varies strongly with $N_e$ and to a lesser extent with $N_\vartheta$ and with Sc. We will discuss the sensitivity of the volume reflectivity in more detail below.

It is important to note that the 'breaks' in the spectra in Fig. 6 vary strongly with kinematic viscosity $v \propto 1/\rho$ and therefore with altitude. The scale corresponding to the break is defined as (see Lübken, 1997):

$$\ell_\circ^H = 9.90 \cdot \eta_{Kol} = 9.90 \cdot \left( \frac{v^3}{\epsilon} \right)^{1/4} \quad (4)$$

EGU

In Fig. 7 we show energy dissipation rates $\epsilon$ and the corresponding heating rates required to fulfill the condition $\ell_o^H = \ell_{Br}$, which is a very rough criterion to allow turbulence producing substantial fluctuations for radar wave scatter. From Eq. (4) we see that $\epsilon \sim \nu^3 \sim 1/\rho^3$, i.e., the required turbulence intensity increases rapidly with altitude. It is obvious from this plot that unrealistic strong turbulence (heating rates of up to 1 million K/d!) would be required to produce fluctuations at VHF radar scales in the upper mesosphere, whereas moderate or even small turbulence (heating rates: 0.1–10 K/d) is sufficient in the lower mesosphere.

We have systematically studied the sensitivity of the volume reflectivity, $\eta$ on electron number densities, $N_e$, turbulent energy dissipation rates, $\epsilon$, Schmidt numbers, $Sc$, and on $N_\vartheta$. The variation of $\eta$ with $N_e^2$ comes from the fact that relative electron density fluctuations are considered in deriving Eqs. (1) and (2), whereas the radar signal comes from absolute electron number density fluctuations. We argue that relative electron (and ion) density fluctuations created by neutral air turbulence are fairly similar in all cases of turbulence, whereas absolute electron density fluctuations can vary substantially depending on the mean background electron density. This idea comes from the simple consideration that the 'mixing ratio' of ions and electrons (relative to neutrals) is constant when an air parcel is moved vertically. Since the background gradient in the plasma is normally different from the neutral atmosphere, relative ion fluctuations ($\Delta N_i/N_i$) are larger compared to neutrals ($\Delta n/n$). Simple scale height considerations lead to the following relationship (see Thrane and Grandal, 1981, for more details):

$$\frac{\Delta N_i}{N_i} = \frac{1}{F} \cdot \frac{\Delta n}{n} \quad ; \quad F = \frac{\gamma \frac{H_p}{H_n} - 1}{\gamma \frac{H_p}{H_i} - 1} \tag{5}$$

where $H_p$, $H_n$ and $H_i$ are the scale heights of pressure, neutral density, and ion density, respectively. Indeed, there have been several in-situ measurements of ion and electron number densities during winter conditions which show fluctuations on the order of 1–5% (much larger than neutral air fluctuations) and conversion factors (1/F) of ap-

proximately 5–10 (Thrane and Grandal, 1981; Thrane et al., 1985, 1994; Lübken et al., 1987, 1993; Blix et al., 1990a,b).

The quantity $N_\vartheta$ determines the total variability of the tracer, together with $N_e$ and $\epsilon$. We have determined $N_\vartheta$ from our neutral air turbulence measurements in 12 sound-
5  ing rocket flights and found typical values of $10^{-8}$ to $10^{-6}$/s. From Eqs. (3) and (5) we see that for electrons the quantity $N_\vartheta$ must be larger by a factor of approximately $1/F^2 \sim 25\ldots100$. We have therefore taken $N_\vartheta = 1 \cdot 10^{-5}$/s as our standard case. This number is compatible with a direct determination of $N_\vartheta$ from a comparison of neutral air and plasma fluctuation spectra (Lübken et al., 1994; Giebeler, 1995).

10  In Fig. 8 we show the volume reflectivity $\eta_{3m}$ calculated from Eq. (2) at $\ell_{Br} = 3$ m. Note that we have used a kinematic viscosity of $\nu = 0.245$ m$^2$/s corresponding to an altitude of 70 km. It is obvious from Fig. 8 that $\eta_{3m}$ varies much stronger with electron density than with Schmidt number. Furthermore, the intensity of turbulence (namely $\epsilon$) plays an important role for $\eta_{3m}$. On the other hand, weak turbulence can be compensated for
15  by large electron number densities. For example, for a volume reflectivity of $\eta = 10^{-15}$/m (typical for PMWE) a decrease of $\epsilon$ from 0.1 to 0.01 W/kg can be compensated for by an increase of $N_e$ from $4 \cdot 10^9$ to $1 \cdot 10^{11}$/m$^3$. It is clear from Fig. 8 that any speculation about the presence of particles based on Schmidt numbers is only meaningful if accompanied by precise measurements of electron number densities and turbulence.

20  We now apply the theoretical considerations from above to our measurements during the ROMA/PMWE campaign. In Fig. 9 the electron density profile measured by the Faraday instrument during flights RWMM01 and RWMM02 are shown together with a simple analytical approximation and extrapolation to altitudes below and above the actual measurements. We also show in that figure a compilation of daytime electron
25  density measurements from rocket borne wave propagation from the auroral zone. The electron densities measured during our PMWE campaign were indeed exceptionally large, in fact the largest in the entire collection of comparable measurements, except for one profile observed at Ft. Churchill during a PCA event. The extended electron density profile from the Faraday measurement during our campaign is used to deter-

EGU

mine the volume reflectivity from Eq. (2) assuming very weak, weak, moderate, and strong turbulence ($\epsilon$=0.001, 0.01, 0.1, and 1 W/kg, respectively), independent of altitude. It is important to note that we have assumed that no particles and no negative ions are present in the atmosphere, i.e., Sc=1. The results are shown in Fig. 10 (left panel). As can be seen, moderate and even weak turbulence can produce a reflectivity of $10^{-14}$–$10^{-13}$/m which is even larger than typical PMWE values (see Fig. 2). We note, however, that the electron densities are significantly larger compared to typical disturbed conditions and to MF and EISCAT measurements prior and after the flight (W. Singer, private communication). We have sketched a more typical electron density profile during disturbed conditions in Fig. 9 which is presumably more representative for general PMWE conditions. The corresponding volume reflectivities are on the order of $10^{-16}$–$10^{-15}$/m (see Fig. 10, right panel), in close agreement with observations.

## 5. Discussion

The volume reflectivities shown in Fig. 10 nicely agree with the mean altitude statistics of PWME with a maximum appearance around 70 km. Assuming that turbulence of various strengths occurs in the entire mesosphere, the height range of PMWE is limited by two effects: viscosity is very large at higher altitudes and dampens all small-scale fluctuations. On the other hand, too few electrons are available below 55 km to allow significant radar backscatter. We note, that the turbulence climatology presented in Lübken (1997) shows rather small turbulence in the winter mesosphere with typical $\epsilon$ values of 0.001–0.01 W/kg. Still, even for weak turbulence the volume reflectivity is large enough to result in PMWE, provided the electron densities are large enough. We should keep in mind that the compilation in Lübken (1997) is based on 12 flights only. It is conceivable that on occasions turbulence can be stronger than in these flights. The maximum volume reflectivity observed by the radar is in quantitative agreement with the estimates presented above assuming turbulence without aerosols.

The turbulence climatology published in Lübken (1997) explains why no echoes are

EGU

observed in the summer lower mesosphere. In summer we have never observed any turbulence below 76 km in a total of 13 flights. The exception to this rule comes from the flights during the summer of 2002 which, however, has been very special in terms of the general atmospheric circulation and wave activity (Goldberg et al., 2004; Becker et al., 2004; Rapp et al., 2004).

There are several indications that turbulence was indeed present during PMWE. The PIP instrument detects small-scale fluctuations of positive ion densities which are a good tracer for neutral air fluctuations. The spectra of these fluctuations (Fig. 5) clearly show strong fluctuations with turbulence spectral characteristics inside the PMWE layer, whereas fluctuations are basically absent outside the layer.

The near-adiabatic temperature profiles shown earlier indicate that turbulence mixing must have been present for a substantial period. In Fig. 11 we show the temperature profiles from flights RWFS16 and RWFS17 together with the radar echoes during that flight, more precisely in a period of approximately 15 min centered around the launch time. There is a region of near-adiabatic lapse rates close to the PMWE layer. The slight mismatch in altitude by a few km can be explained by a small tilt of the layers by ~0.1 km/km. We note that a steep temperature gradient is also present in the lidar profile shown in Stebel et al. (2004) in the case that no aerosols are present ('Alternative 2' in their Fig. 4).

The apparent absence of radar echoes in the center of the turbulent layer during flight RWFS17 is in perfect agreement with the theory of Fritts et al. (2003) and has been observed for other tracers in the troposphere (see Fig. 5 in the Fritts et al. paper). The explanation of this effect is that persistent turbulent mixing destroys the background gradient of the tracer and thereby inhibits the generation of fluctuations even if turbulence is still active.

Another indication for turbulence comes from the Richardson numbers in Fig. 4 which indicate unstable regions (i.e., $Ri$ smaller as 1/4) at PMWE altitudes and above. In general, regions of PMWE seen in Fig. 1 agree with the appearance of instability observed in Fig. 4. For example, $Ri$ is very low at roughly 60–65 km altitude, where strong radar

EGU

echoes are observed. A one-to-one relationship cannot be expected due to the patchy and intermittent character of turbulence, the time constants of turbulence production and destruction, and the horizontal difference between the radar volume and the rocket probing. We note that recent model simulations of gravity wave breaking have shown
5  that turbulence can be generated even if the Richardson number is significantly larger than unity (Achatz and Schmitz, 2005).

Further evidence for turbulence at PMWE altitudes comes from the spectral width of the radar echo shown in Fig. 12. Large spectral broadening corresponding to velocity fluctuations of up to $\sigma_{obs} \sim 10$ m/s are observed within PMWE. We hesitate to convert
10  these values to turbulence parameters since part of the observed broadening might be due to instrumental effects such as beam and shear broadening (Hocking, 1983). We have used a typical horizontal wind speed from our falling sphere flights of v$\sim$60 m/s to roughly estimate the instrumental broadening and arrive at $\sigma_{instr} \sim$v$\cdot \sin(2.55°) \sim 2.7$ m/s. Using $\sigma_{turb} = \sqrt{\sigma_{obs}^2 - \sigma_{instr}^2}$ this leads to somewhat smaller turbulent broadening, $\sigma_{turb}$.
15  However, a significant part of the observed broadening is caused by atmospheric velocity fluctuations presumably caused by turbulence. We note that we cannot study the aspect sensitivity of backscatter since only the vertical beam was in operation during the campaign.

Our falling sphere temperature measurements clearly show that the atmospheric
20  temperature is much larger than the frost point temperature (by more than 50 K). In other words, it is much too warm to allow the existence of water ice particles. The question remains whether other 'large' charged particles are present which could influence the radar backscatter. The observations and the theoretical considerations presented above did not give any evidence for aerosol particles. Contrary to the sum-
25  mer mesopause region, particles are not needed to explain the winter echoes. On the other hand, from our measurements we cannot positively exclude that particles are present. Certainly, they cannot be large (radius larger than 20–30 nm) because they would then cause a significant enhancement in the lidar signal. Schmidt numbers significantly larger than unity indicate the presence of charged particles and have indeed

Print Version

Interactive Discussion

EGU

**Polar mesosphere winter echoes**

F.-J. Lübken et al.

been determined from in-situ measurements of neutral and plasma fluctuations in the vicinity of summer echoes (Lübken et al., 1994). Similar attempts would be rather difficult for the winter echoes since the Schmidt number is presumably much smaller than in summer because particles are smaller (see above).

5    We note that the presence of a sufficiently large number of negative ions will take care of the charge balance with positive ions and will thereby enhance the mobility of free electrons (Stebel et al., 2004; Hill, 1978). This would lead to Schmidt numbers smaller than one. We have not considered this case since daylight and particle precipitation prohibits the attachment of electrons to form negative ions. Wether or not a

10   sufficient number of negative ions can form during night under geomagnetic disturbed conditions is not yet clear. We note, that no electron or negative ion density measurements have been performed during night in the presence of PMWE.

Apart from turbulence the most crucial requirement for PMWE is a sufficiently large electron number density. During disturbed conditions precipitating particles from the

15   Sun or from the Earth's magnetosphere create electron number densities which can be orders of magnitude larger compared to normal conditions. During night part of these electrons are attached to neutrals to form negative ions. These electrons are immediately detached by solar radiation once the Sun rises or when proton/electron precipitation occurs. This explains why PMWE are (nearly) only observed during the

20   day and during strong disturbance, such as solar proton events. From Fig. 9 we see that electron densities can vary by several orders of magnitude depending on the source strength (solar/geomagnetic) and on other factors involving ion-chemistry and photochemistry. The sources and sinks cannot be modeled accurately enough to predict the electron profile for all conditions with sufficient accuracy. Therefore, a precise theoret-

25   ical prediction of volume reflectivity from turbulence requires a precise measurements of electron number densities, e.g. by the Faraday rotation technique.

EGU

## 6. Summary and conclusions

Various experimental observations support the idea that PMWE during the ROMA/PMWE campaign are caused by neutral turbulence, namely

- – The spectrum of ion density fluctuations shows turbulence like characteristics within PMWE, and no fluctuations outside PMWE.

- – Persistent steep temperature gradients close to the adiabatic lapse rate in the vicinity of the PMWE layer indicate turbulent mixing. In one case we observe a text book example of fluctuations at the edges of the turbulent layer in agreement with theory.

- – Temperature measurements from FS and high resolution wind measurements by chaff show very low Richardson numbers indicating instability.

- – Spectral broadening of the VHF signal indicates velocity fluctuations of several m/s, presumably due to turbulence.

- – Turbulence explains the general altitude dependence of PMWE with a maximum around 70 km (too large viscosity above 80 km and too few electrons below 60 km).

- – Volume reflectivities calculated from turbulence theory agrees quantitatively with observations.

- – The seasonal variation of turbulence explains the non-existence of echoes in the summer lower mesosphere.

We have based our general considerations about turbulent PMWE on as many measurements of turbulent parameters as available, in particular regarding $\epsilon$ and $N_\vartheta$. Other studies hinge on uncertain estimates of 'constants' which are only poorly known and further suffer from idealistic assumptions of turbulence generation etc. Since this leads

EGU

EGU

to uncertainties in the calculated volume reflectivities of several orders of magnitude, a relatively small discrepancy between measured and theoretical values of $\eta$ cannot be used to rule out turbulence as a cause of PMWE.

Our observations and theoretical considerations show that particles are not needed to explain PMWE (as opposed to summer echoes). On the other hand, we cannot positively exclude their existence from our data as long as they are smaller than $\sim$20 nm. We have stated earlier that any speculation about the presence of particles based on Schmidt numbers is only meaningful if accompanied by precise measurements of electron number density and turbulence. Since Sc is small and PMWE occurrence is low, this will be a very difficult task. It is presumably easier to detect these particles directly by in-situ techniques as is planned in several projects in the near future.

## References

Achatz, U. and Schmitz, G.: Shear and Convective Instability of Inertia-Gravity Wave Packets: Modal and Nonmodal Growth, J. Atmos. Sci., in print, 2005. 7626

Becker, E., Müllemann, A., Lübken, F.-J., Körnich, H., Hoffmann, P., and Rapp, M.: High Rossby-wave activity in austral winter 2002: Modulation of the general circulation of the MLT during the MaCWAVE/MIDAS northern summer program, Geophys. Res. Lett., 31, doi:10.1029/2004GL019615, 2004. 7625

Blix, T. A., Thrane, E. V., and Andreassen, Ø.: In-situ measurements of fine-scale structure and turbulence in the mesosphere and lower thermosphere by means of electrostatic positive ion probes, J. Geophys. Res., 95, 5533–5548, 1990a. 7623

Blix, T. X., Thrane, E. V., Fritts, D. C., von Zahn, U., Lübken, F.-J., Hillert, W., Blood, S. P., Mitchell, J. D., Kokin, G. A., and Pakhomov, S. V.: Small scale structure observed in-situ during MAC/EPSILON, J. Atmos. Terr. Phys., 52, 835–854, 1990b. 7623

Czechowsky, P., Rüster, R., and Schmidt, G.: Variations of mesospheric structures in different seasons, Geophys. Res. Lett., 6, 459–462, 1979. 7615

Driscoll, R. J. and Kennedy, L. A.: A model for the spectrum of passive scalars in an isotropic turbulence field, Phys. Fluids, 28, 72–80, 1985. 7620

Ecklund, W. L. and Balsley, B. B.: Long-term observations of the Arctic mesosphere with the MST radar at Poker Flat, Alaska, J. Geophys. Res., 86, 7775–7780, 1981. 7615

Friedrich, M., Harrich, M., Steiner, R. J., Torkar, K. M., and Lübken, F.-J.: The quiet auroral ionosphere and its neutral background, Adv. Space Res., 33, 943–948, 2004. 7617

Fritts, D. C., Bizon, C., Werne, J., and Meyer, C.: Layering accompanying turbulence generation due to shear instability and gravity wave breaking, JGR, 108(D8), 8452, doi:10.1029/2002JD002406, 2003. 7625

Giebeler, J.: In-situ Messungen zur Untersuchung der Rolle von Turbulenz bei der Erzeugung von Radarechos in der polaren Mesosphäre im Sommer, PhD thesis, Bonn University, BONN-IR-95-28, 1995. 7620, 7623

Goldberg, R. A., Fritts, D. C., Williams, B. P., Lübken, F.-J., Rapp, M., Singer, W., Latteck, R., Hoffmann, P., Müllemann, A., Baumgarten, G., Schmidlin, F. J., She, C.-Y., and Krueger, D. A.: The MacWAVE/MIDAS rocket and ground-based measurement of polar summer dynamics: overview and mean state structure, Geophys. Res. Lett., 31, doi:10.1029/2004GL019411, 2004. 7625

Hill, R. J.: Nonneutral and quasi-neutral diffusion of weakly ionized multiconstituent plasma, J. Geophys. Res., 83, 989–998, 1978. 7627

Hocking, W. K.: On the extraction of atmospheric turbulence parameters from radar backscatter Doppler spectra – I. Theory, J. Atmos. Terr. Phys., 45, 89–102, 1983. 7626

Kirkwood, S., Barabash, V., Belova, E., Nilsson, H., Rao, T. N., Stebel, K., Osepian, A., and Chilson, P. B.: Polar Mesosphere Winter Echoes during Solar Proton Events, Adv. Polar Upper Atmos. Res., 16, 111–125, 2002. 7615, 7618

Kirkwood, S., Belova, E., Dalin, P., Fricke, K.-H., Blum, U., Schmidlin, F., and Goldberg, R. A.: Polar Mesosphere winter echoes during MaCWAVE, in: Proceedings of the 16th ESA Symposium on European Rocket and Balloon Programmes and Related Research, St. Gallen, Switzerland, edited by: Warmbein, B., vol. ESA SP-530, pp. 357–362, 2003. 7619

**Polar mesosphere winter echoes**

F.-J. Lübken et al.

Title Page

| Abstract | Introduction |
| Conclusions | References |
| Tables | Figures |

◀◀   ▶▶

◀   ▶

Back   Close

Full Screen / Esc

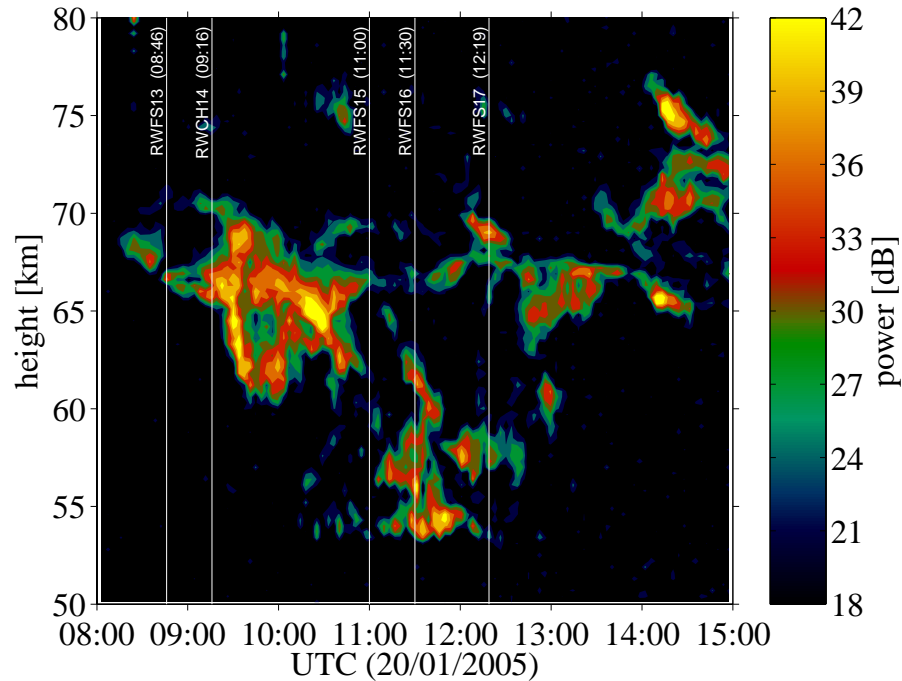Print Version

Interactive Discussion

EGU

Latteck, R., Singer, W., and Bardey, H.: The ALWIN MST radar – Technical design and performances, in: Proceedings of the 14th ESA Symposium on European Rocket and Balloon Programmes and Related Research, Potsdam, Germany, edited by: Kaldeich-Schürmann, B., vol. ESA SP-437, pp. 179–184, 1999.  7616

Lübken, F.-J.: On the extraction of turbulent parameters from atmospheric density fluctuations, J. Geophys. Res., 97, 20 385–20 395, 1992.  7621

Lübken, F.-J.: Seasonal variation of turbulent energy dissipation rates at high latitudes as determined by in-situ measurements of neutral density fluctuations, J. Geophys. Res., 102, 13 441–13 456, 1997.  7621, 7624

Lübken, F.-J.: Thermal structure of the Arctic summer mesosphere, J. Geophys. Res., 104, 9135–9149, 1999.  7617

Lübken, F.-J. and von Zahn, U.: Thermal structure of the mesopause region at polar latitudes, J. Geophys. Res., 96, 20 841–20 857, 1991.  7619, 7636

Lübken, F.-J., von Zahn, U., Thrane, E. V., Blix, T., Kokin, G. A., and Pachomov, S. V.: In-situ measurements of turbulent energy dissipation rates and eddy diffusion coefficients during MAP/WINE, J. Atmos. Terr. Phys., 49, 763–775, 1987.  7623

Lübken, F.-J., Hillert, W., Lehmacher, G., and von Zahn, U.: Experiments revealing small impact of turbulence on the energy budget of the mesosphere and lower thermosphere, J. Geophys. Res., 98, 20 369–20 384, 1993.  7623

Lübken, F.-J., Giebeler, J., Blix, T., Thrane, E., Singer, W., and Bremer, J.: In-situ measurement of the Schmidt number within a PMSE layer, Geophys. Res. Lett., 21, 1651–1654, 1994.  7620, 7623, 7627

Mechtly, E. A., Bowhill, S. A., Smith, L. G., and Knoebel, H. W.: Lower ionosphere electron concentrations and collision frequency from rocket measurements of Faraday rotation, differential absorption, and probe current, J. Geophys. Res., 72, 5239–5245, 1967.  7617

Rapp, M. and Lübken, F.-J.: Polar mesosphere summer echoes (PMSE): Review of observations and current understanding, Atmos. Chem. Phys., 4, 2601–2633, 2004, SRef-ID: 1680-7324/acp/2004-4-2601.  7615

Rapp, M., Strelnikov, B., Müllemann, A., Lübken, F.-J., and Fritts, D. C.: Turbulence measurements and implications for gravity wave dissipation during the MacWave/MIDAS rocket program, Geophys. Res. Lett., 31, doi:10.1029/2003GL019325, 2004.  7625

Schmidlin, F. J.: The inflatable sphere: A technique for the accurate measurement of middle atmosphere temperatures, J. Geophys. Res., 96, 22 673–22 682, 1991.  7617

EGU

Stebel, K., Blum, U., Fricke, K.-H., Kirkwood, S., Mitchell, N. J., and Osepian, A.: Joint radar/lidar observations of possible aerosol layers in the winter mesosphere, J. Atmos. Solar Terr. Phys., 66, 957–970, 2004. 7615, 7619, 7625, 7627

Strelnikov, B., Rapp, M., and Lübken, F.-J.: A new technique for the analysis of neutral air density fluctuations measured in situ in the middle atmosphere, Geophys. Res. Lett., 30, doi:10.1029/2003GL018271, 2003. 7620

Tatarskii, V. I.: Wave propagation in a turbulent medium, McGraw-Hill Book Comp., New York, 1961. 7620

Thrane, E., Blix, T., Hoppe, U.-P., Lübken, F.-J., Hillert, W., Lehmacher, G., and Fritts, D.: A study of small-scale waves and turbulence in the mesosphere using simultaneous in-situ observations of neutral and plasma fluctuations, J. Atmos. Terr. Phys., 56, 1797–1808, 1994. 7623

Thrane, E. V. and Grandal, B.: Observations of fine scale structure in the mesosphere and lower thermosphere, J. Atmos. Terr. Phys., 43, 179–189, 1981. 7622, 7623

Thrane, E. V., Andreassen, Ø., Blix, T., Grandal, B., Brekke, A., Philbrick, C. R., Schmidlin, F. J., Widdel, H.-U., von Zahn, U., and Lübken, F.-J.: Neutral air turbulence in the upper atmosphere observed during the Energy Budget Campaign, J. Atmos. Terr. Phys., 47, 243–264, 1985. 7623

Torrence, C. and Compo, G. P.: A practical guide to wavelet analysis, Bull. Amer. Meteor. Soc., 79, 61–79, 1998. 7620

Widdel, H. U.: Foil chaff clouds as a tool for in-situ measurements of atmospheric motions in the middle atmosphere: Their flight behaviour and implications for radar tracking, J. Atmos. Terr. Phys., 52, 89–101, 1990. 7617

**Polar mesosphere winter echoes**

F.-J. Lübken et al.

EGU

**Table 1.** Rockets launched during the ROMA/PMWE campaign in 2005.

| date | time (UT) | label |
| --- | --- | --- |
| 18 Jan. | 11:36:30 | RWMM01 |
| ” | 12:06:00 | RWMM02 |
| ” | 12:36:00 | RWFS03 |
| ” | 13:15:00 | RWFS04 |
| ” | 13:58:00 | RWCH05 |
| ” | 14:42:00 | RWFS06 |
| ” | 15:31:00 | RWFS07 |
| ” | 16:07:00 | RWCH08 |
| ” | 16:54:00 | RWFS09 |
| ” | 17:24:00 | RWFS10[1)] |
| ” | 17:57:00 | RWCH11 |
| ” | 18:35:00 | RWFS12 |
| 20 Jan. | 08:46:00 | RWFS13 |
| ” | 09:16:00 | RWCH14 |
| ” | 11:00:00 | RWFS15 |
| ” | 11:30:00 | RWFS16 |
| ” | 12:19:00 | RWFS17 |
| 21 Jan. | 13:06:00 | RWFS18 |
| 25 Jan. | 01:30:00 | RWFS19 |
| ” | 03:30:00 | RWFS20 |
| ” | 05:30:00 | RWFS21 |
| ” | 07:30:00 | RWFS22 |
| 27 Jan. | 12:22:00 | RWFS23 |

RW = ROMA/Winter, FS = falling sphere, CH = chaff
MM = Mini-Midas; [1)] RWFS10 was a failure

Title Page

Abstract | Introduction

Conclusions | References

Tables | Figures

◄ | ►I

◄ | ►

Back | Close

Full Screen / Esc

Print Version

Interactive Discussion

EGU

**Fig. 1.** Backscatter power in dB above noise level detected by the ALWIN VHF radar on 20 January 2005, from 08:00–15:00 universal time (=09:00–16:00 local time). The vertical lines indicate launch times of falling spheres.

**Polar mesosphere winter echoes**

F.-J. Lübken et al.

EGU
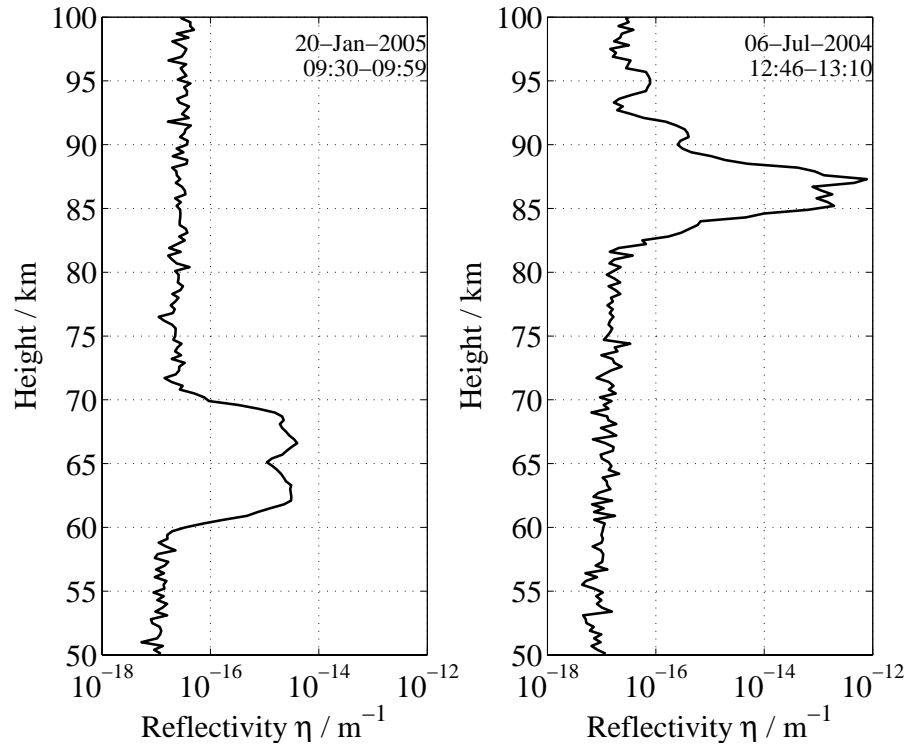


**Fig. 2.** Volume reflectivities deduced from the ALWIN radar backscatter power for a typical winter echo from 20 January 2005 (left panel), and for a summer echo on 6 July 2004 (right panel). In both cases the radar signal was averaged for ∼1/2 h.
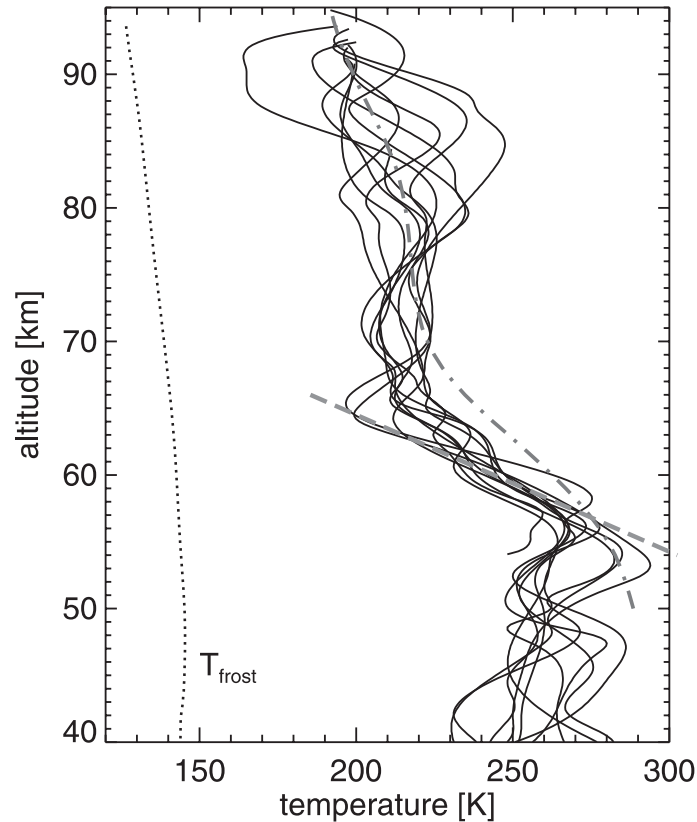
**Fig. 3.** Temperature profiles from falling spheres in the presence of PMWE. Profile from flights RWFSxx, xx=03, 04, 06, 07, 09, 12, 13, 15, 16, 17, 18 are shown (see Table 1 for more details). The dotted line shows the frost point temperature. The dashed-dotted line is the mean January temperature profile from the FS climatology of Lübken and von Zahn (1991). The dashed line indicates an adiabatic temperature lapse rate of −9.8 K/km.
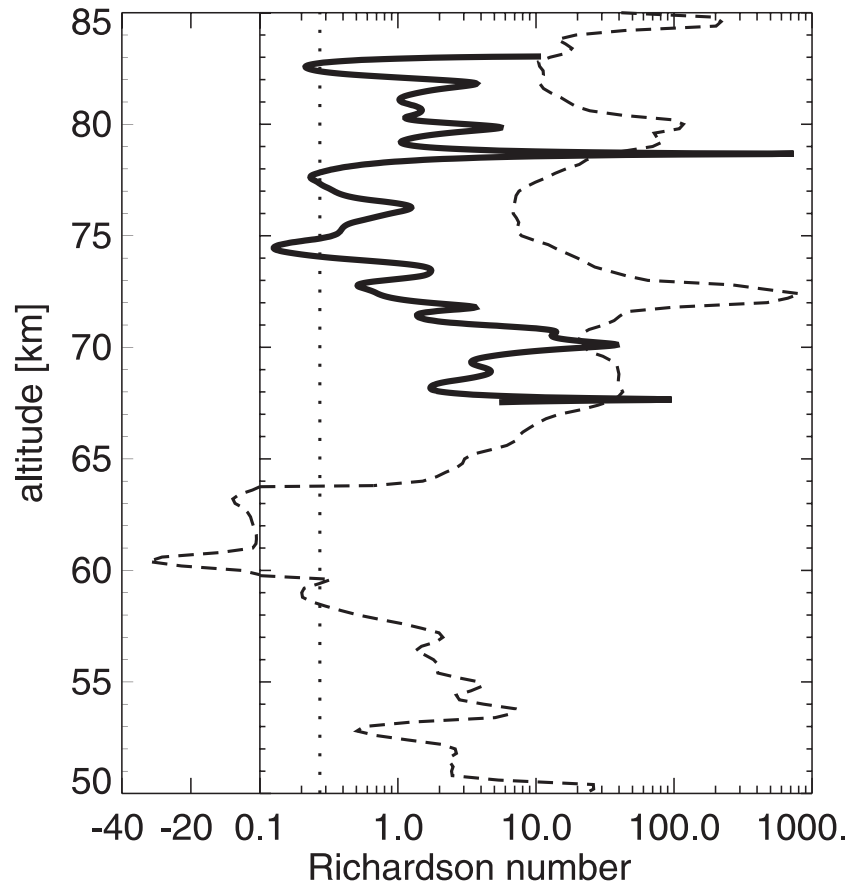
**Fig. 4.** Richardson number calculated from the chaff winds (RWCH14) and falling sphere temperatures (RWFS17, solid line). Dashed line: same but using winds and temperatures from falling sphere (RWFS17). Note the change of scales for negative $Ri$ numbers. The dotted vertical indicates $Ri = 1/4$.

EGU
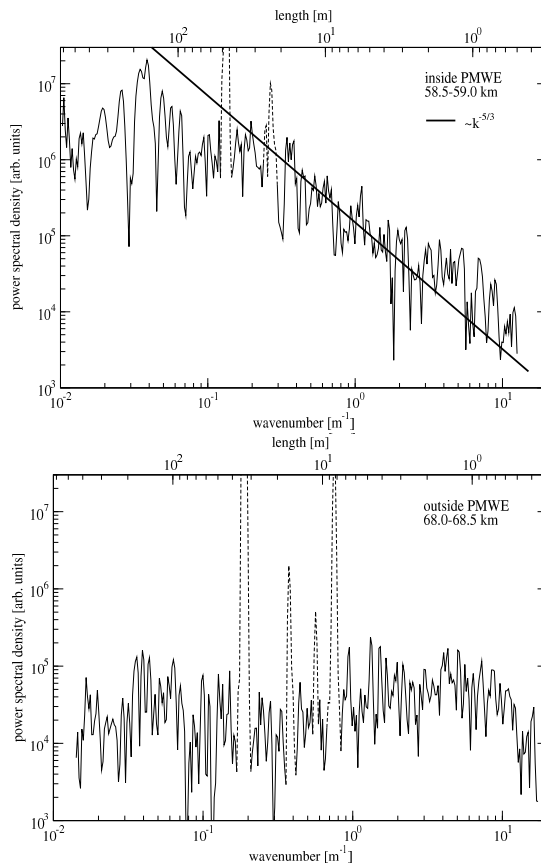
**Fig. 5.** Power spectral density of relative ion fluctuations as measured by the PIP instrument during flight RWMM01. Upper panel: spectrum from an altitude range within PMWE. The straight line indicates a –5/3 power law expected from classical turbulence theory. Lower panel: spectrum from an altitude range without PMWE. The prominent peaks in the spectra (dashed lines) are caused by the payload spin frequency and its harmonics.

Title Page

Abstract | Introduction

Conclusions | References

Tables | Figures

|◄ | ►|

◄ | ►

Back | Close

Full Screen / Esc

Print Version

Interactive Discussion

EGU
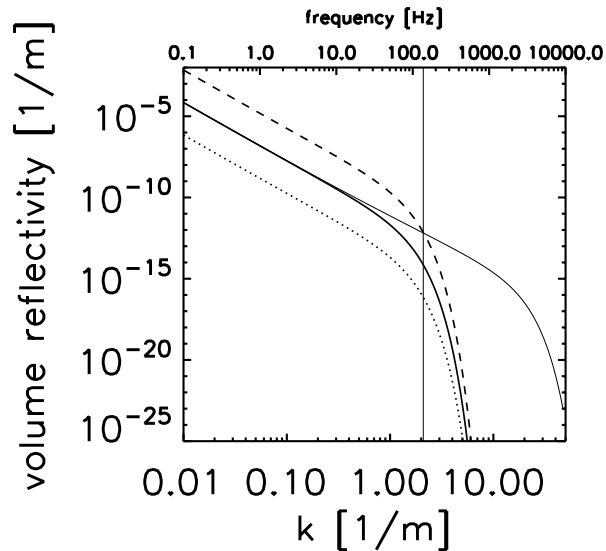
**Fig. 6.** Volume reflectivity as a function of wave number for various cases of electron densities $N_e$, Schmidt number Sc, and $N_\vartheta$. Standard case (thick solid curve): $N_e$=1·10$^{10}$/m$^3$, $N_\vartheta$ =1·10$^{-5}$/s, and Sc=1. Relative to the standard case the electron density has been decreased by a factor of 10 (dotted line), $N_\vartheta$ has been increased by the factor of 100 (dashed line), and the Schmidt number has been increased by a factor of 100 (thin solid line). The energy dissipation rates is $e$=0.1 W/kg and the kinematic viscosity is $\nu$=0.245 m$^2$/s for all curves. The value for $\nu$ is representative for an altitude of 70 km. The thin vertical line corresponds to the Bragg scale of the ALWIN radar.

EGU

EGU
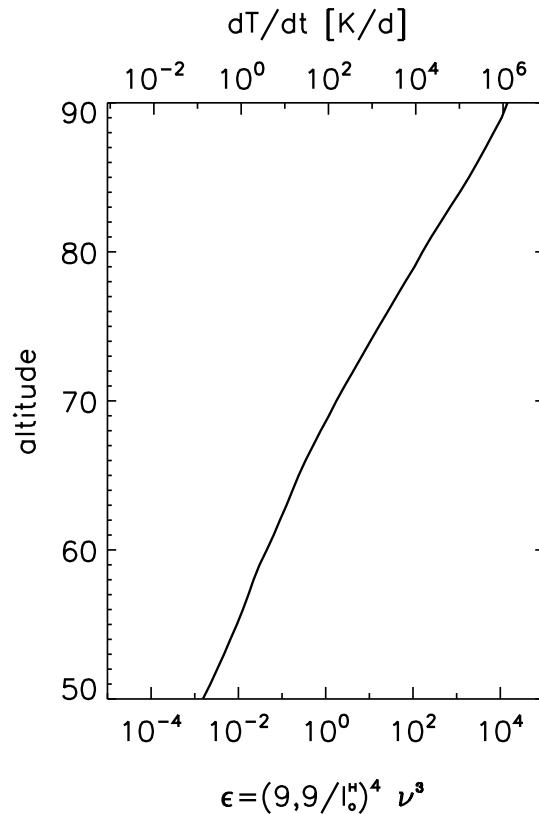


**Fig. 7.** Turbulent energy dissipation rates derived from the condition $\ell_o^H = \ell_{Br}$ ($\ell_{Br} = 3$ m) which is a very rough criterion to allow turbulence producing substantial fluctuations for radar wave scatter. The upper axis shows the corresponding heating rates calculated from $dT/dt = \epsilon/c_p$ ($c_p$ = heat capacity of air at constant pressure).

**Polar mesosphere winter echoes**

F.-J. Lübken et al.
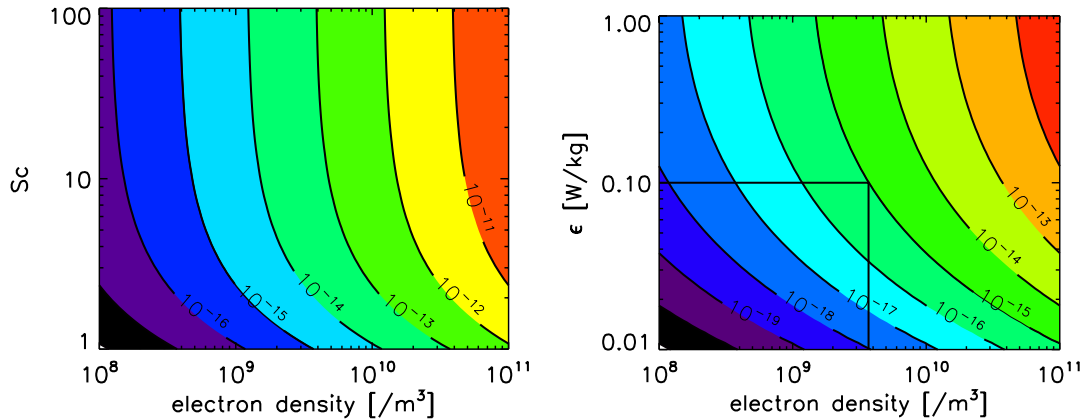
**Fig. 8.** Left panel: The sensitivity of the volume reflectivity at 3 m to changes in electron density and Schmidt number for $\epsilon$=0.1 W/kg and $N_{\vartheta}$=1·$10^{-5}$/s. Right panel: Same, but for electron density and turbulent energy dissipation rate (Sc=1 ; $N_{\vartheta}$=1·$10^{-5}$/s). A kinematic viscosity of $\nu$=0.245 $m^2$/s is used, representative for an altitude of 70 km.

EGU

EGU
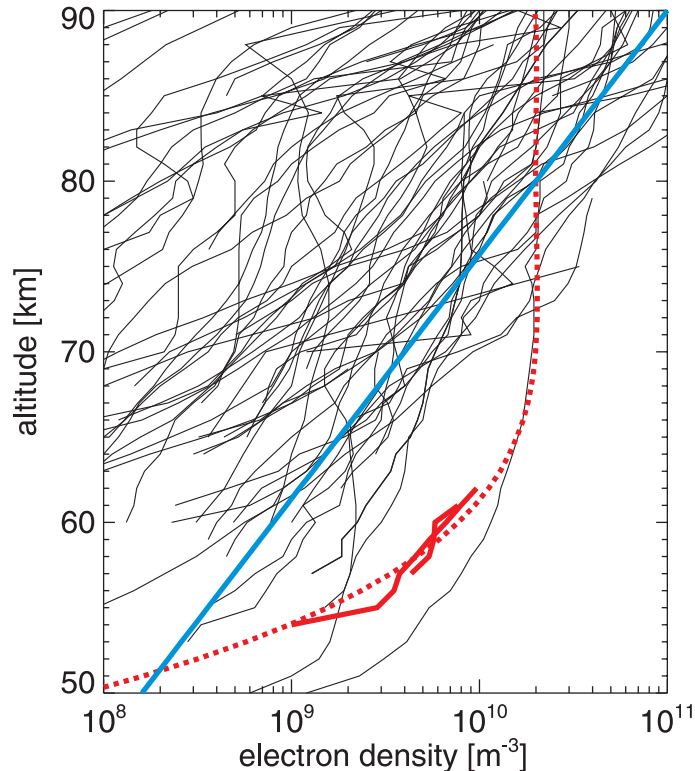
**Fig. 9.** Electron density profiles measured by the Faraday technique in flights RWMM01 and RWMM02 (thick red lines), pragmatically extended to larger and smaller altitudes (red dotted line). We also show a compilation of daytime electron density measurements from the Faraday technique from the auroral zone (thin lines) and a straight line representing 'typical' electron densities during disturbed conditions (blue line).

**Polar mesosphere winter echoes**

F.-J. Lübken et al.
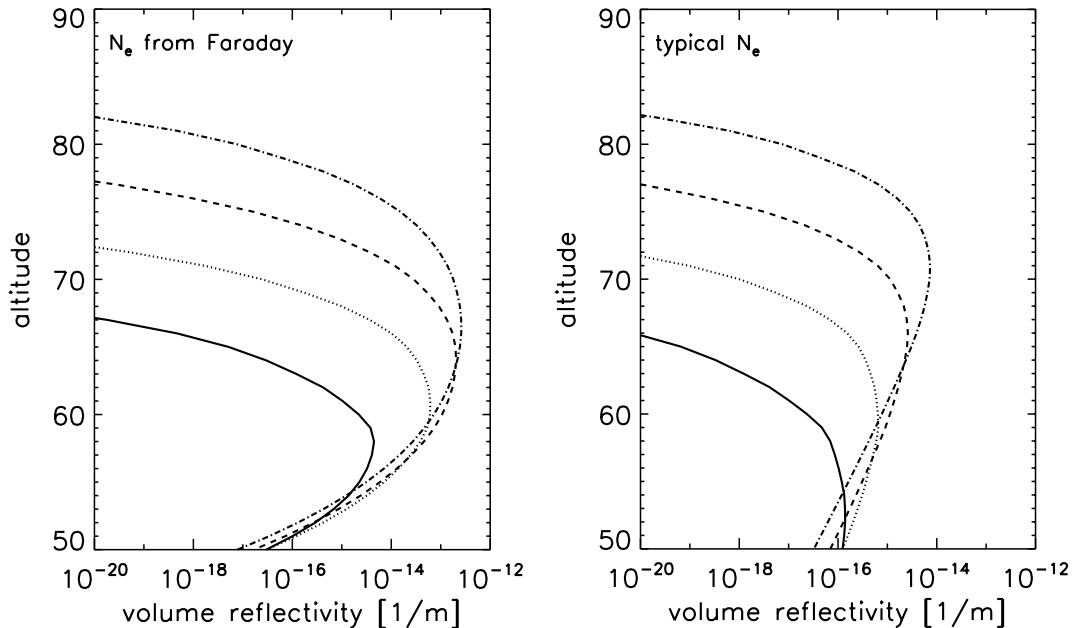
**Fig. 10.** Left panel: Volume reflectivity at the ALWIN radar Bragg scale for various turbulence strength, namely $\varepsilon=0.001$ (solid), $=0.01$ (dotted), $=0.1$ (dashed), and 1. (dashed-dotted). All values in W/kg. The electron density profile from the extended Faraday profile in Fig. 9 has been used. Right panel: Same as left panel but with 'typical' electron profile from Fig. 9. For all profiles we have used $N_{\vartheta}=1\cdot10^{-5}$/s.
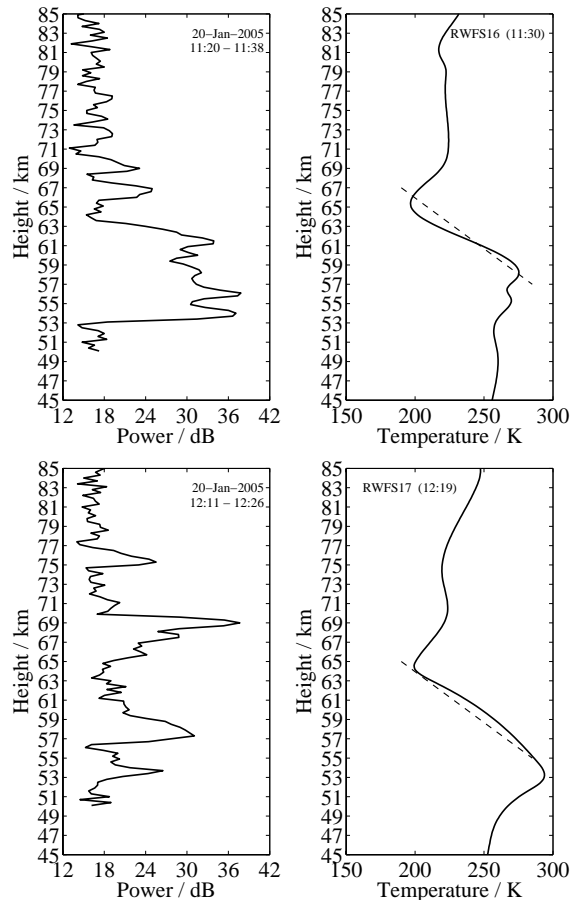
EGU

**Fig. 11.** Comparison of temperature profiles (right panels) with radar power profiles (left panels) for flights RWFS16 and RWFS17. The radar signal was averaged for a time period of ~15 min, roughly centered at the launch time. The dashed lines indicate an adiabatic lapse rate.

Title Page

Abstract    Introduction

Conclusions    References

Tables    Figures

◄    ►|

◄    ►

Back    Close

Full Screen / Esc

Print Version

Interactive Discussion

EGU
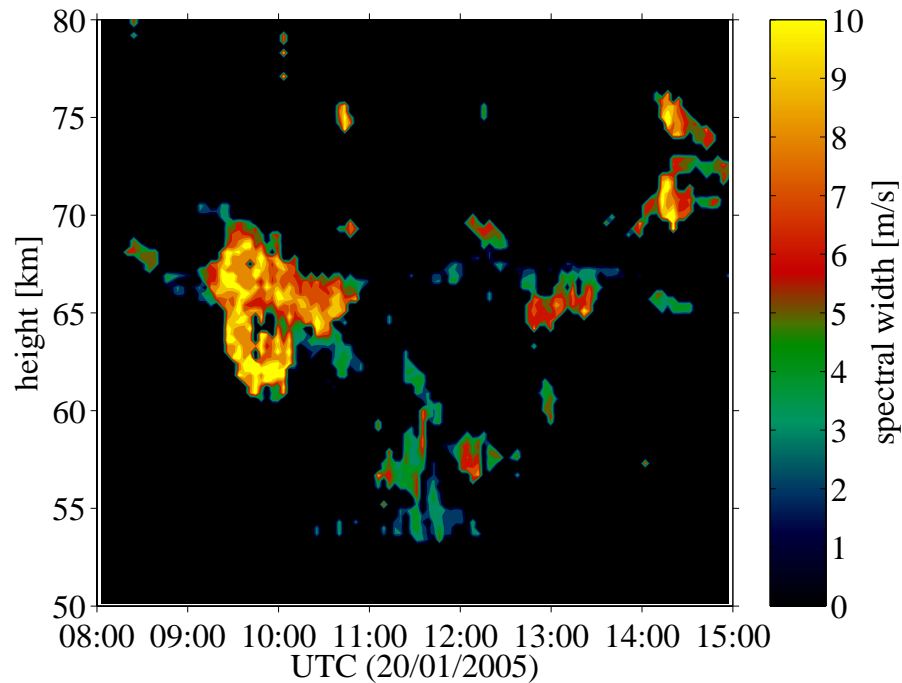
**Fig. 12.** Spectral width of the radar signal expressed in m/s for the PMWE shown in Fig. 1.

Print Version

Interactive Discussion

EGU